

## Drought monitoring in Burdur Lake, Turkey using multi-sensor remote sensing data sets

Ahmet Batuhan Polat\*, Ozgun Akcay, Fazli Kontas

Çanakkale Onsekiz Mart University, Çanakkale, Turkey

e-mail: [abpolat@comu.edu.tr](mailto:abpolat@comu.edu.tr); ORCID: <http://orcid.org/0000-0002-7495-1998>

e-mail: [akcay@comu.edu.tr](mailto:akcay@comu.edu.tr); ORCID: <http://orcid.org/0000-0003-0474-7518>

e-mail: [fazlikontas52@gmail.com](mailto:fazlikontas52@gmail.com); ORCID: <http://orcid.org/0000-0002-1966-3862>

\*Corresponding author: Ahmet Batuhan Polat, e-mail: [abpolat@comu.edu.tr](mailto:abpolat@comu.edu.tr)

Received: 2023-03-27 / Accepted: 2023-10-23

**Abstract:** Water levels in freshwater resources have been descending daily as global temperatures have risen and a coastal recession has occurred. The losses in these water basins have a significant influence on natural life. While drought is a global environmental issue, its consequences may be seen in Turkey. This study looks at the loss of water areas in Burdur Lake, one of Turkey's major lakes, between 2010 and 2021. The areas were identified using supervised classification, and the classification process was carried out for 2010, 2013, 2016, 2019, and 2021, respectively. Furthermore, several drought detection metrics, such as land surface temperature, soil moisture values, Normalized Vegetation Index (NDVI), Enhanced Vegetation Index (EVI), Palmer Drought Severity Index (PDSI), and precipitation amounts, have been evaluated for the study area between 2010 and 2021. The values of all drought detection indicators were also evaluated monthly for each year of the study. The analysis reveals abnormalities in all parameters, particularly in recent years, when compared to earlier years. Water areas decreased by 36.48% as a result of the classifications, whereas sandy areas increased by 89.85%. Again, the average values of various parameters used for drought detection over the years were compared. As a result, the indicator parameters gave reliable results as well as a means of monitoring the drought.

**Keywords:** ecology, land surface temperature, satellite imagery, lake monitoring, Earth observation

### 1. Introduction

In recent years, global warming has been highlighted as the most serious ecological threat to the Earth's surface, with a direct negative impact on life in a variety of ecosystems (Vezzulli et al., 2015; Abirami et al., 2021; Alfonso et al., 2021). Water losses along coastlines and evaporation in water regions are exacerbated by an increase in surface temperature compared to previous years (Woolway et al., 2020).



The Author(s). 2024 Open Access. This article is distributed under the terms of the Creative Commons Attribution 4.0 International License (<http://creativecommons.org/licenses/by/4.0/>), which permits unrestricted use, distribution, and reproduction in any medium, provided you give appropriate credit to the original author(s) and the source, provide a link to the Creative Commons license, and indicate if changes were made.

Meteorological drought is a dynamic situation caused by a lack of precipitation that naturally creates a hydrological imbalance in the landscape as a serious consequence (Trenberth et al., 2014; Pachauri et al., 2021). Drought also has negative impacts on agriculture, the economy, ecosystems, and society (Daryanto et al., 2016; Abbasian et al., 2021). Prolonged droughts lead to disasters such as death, famine, or mass migration in some countries (Wilhite, 2005; Godfray et al., 2010). Droughts in actively flowing waterways, such as groundwater and rivers, also harm energy output in these areas (van Loon, 2015).

Remote sensing methods are frequently used in watersheds to actively monitor drought and take precautions (AghaKouchak et al., 2015; Varghese et al., 2018; Shorachi et al., 2022). Especially in recent years, satellite images with high spatial and temporal resolution have been used to precisely monitor changing water levels due to different factors (Rojas et al., 2011; Hu et al. 2019). In addition to drought monitoring, predictive modeling studies were conducted to assess the effects of future droughts (Park et al., 2018; Feng et al., 2019).

The United Nations has established Sustainable Development Goals (SDGs) that must be achieved by 2030 in order to create a more livable world. A comprehensive assessment of the impacts of climate change and the solutions that can be found is provided in the 13th SDG, "Climate Action". According to this report, drought will be a factor that could force 700 million people to migrate by 2030. Within the framework of the SDGs, there are remote sensing studies that demonstrate the impact of drought on water resources (Bhaga et al., 2020). In this study, the utility of different drought indices for detection was investigated and demonstrated. As a result, they emphasized the effectiveness of Landsat-8 and Sentinel-2 in drought detection using remote sensing methods. The active use of remote sensing methods in alignment with the goal is appropriate for monitoring and taking emergency actions.

Google Earth Engine (GEE) is commonly used for drought monitoring. [12]Benzouagh et al. (2022) conducted a study on the water level in a dam over a seven-year period and utilized the Normalized Difference Water Index (NDWI) to analyze water surfaces. Their findings suggest that water withdrawals can be identified using satellite images, and these conclusions can be validated by various drought parameters. Another GEE study emphasized the significance of LST and NDVI data in drought monitoring (Zhao et al., 2021). It is claimed that while assessing vegetation health, real-time monitoring of NDVI data can provide information about the region's dryness. [22]Ghazaryan et al. (2020) examined drought in agricultural products over a 3-year period using various parameters such as NDVI, LST, and Normalized Difference Moisture Index (NDMI). They also supported their findings with Sentinel-1 Synthetic Aperture Radar backscatter values and found that different parameters respond differently to drought conditions.

Due to the fact that some high-resolution satellite images are only commercially available, moderate-resolution and open-access satellite images, such as Landsat and Sentinel, have also been productively utilized in various environmental studies (Pan et al., 2020). The Landsat series of satellites have found applications in a variety of fields, including heat-sensitive sensing applications, land cover mapping, damage detection, and land change analysis, owing to the multi-band system's sensitivity to multiple spectral

bands, such as thermal and multispectral (Roy et al., 2015; Liu et al., 2018; Alam et al., 2020; Shamsuzzoha et al., 2021). In this study, Landsat 4 and 5 satellite images were used for the year 2010, while Landsat 8 satellite images were used for the years between 2013 and 2021.

One of the most commonly used methods in remote sensing studies is image classification. Satellite image classification is a powerful technique used for extracting information from images (Abburu and Golla, 2015). Classification in remote sensing can be categorized into two main types: unsupervised and supervised classification. Unsupervised classification does not require prior knowledge of the region (Mohammady et al., 2015), resulting in quicker results in terms of the implementation timeline. In contrast, supervised classification necessitates having class information in the satellite image beforehand and defining training samples (Domadia and Zaveri, 2011), essentially teaching specific information to the algorithm during the classification process. It is commonly observed that supervised classification methods tend to yield higher overall accuracy compared to unsupervised approaches (Yiqiang et al., 2010; Batur and Maktav, 2012; Sabuncu and Sunar, 2017). In this study, the Maximum Likelihood approach, which is a supervised classification method, was employed, and the findings were examined in this context.

The Land Surface Temperature (LST) parameter is derived from the thermal bands of satellite images and represents temperature values within a specific time frame in a given region (Cristóbal et al., 2018). The most commonly used satellites for obtaining LST through remote sensing methods are Landsat 8 and MODIS, using the corresponding bands (Avdan and Jovanovska, 2016; Long et al. 2020). These satellites can also reveal correlations between drought and LST in a particular region (Swain et al., 2011). In another study conducted in Turkey, LST and vegetation indices were simultaneously assessed around Salt Lake, revealing a consistent relationship between these values over the years (Orhan et al., 2014). Water losses in large lakes can be associated with LST in general.

Another crucial parameter employed in drought analysis is soil moisture (Yan et al., 2006). Soil moisture levels tend to be higher during seasons with heavy rainfall and lower during periods of low rainfall, often referred to as dry seasons (Kar and Kumar, 2019). The reduced soil moisture resulting from drought conditions can lead to inadequate nourishment of vegetation, causing it to dry out prematurely (Lian et al., 2020). Consequently, this premature drying of plants may increase the risk of unexpected fires (Sazib et al., 2021). Since the 1970s, remote sensing methods have been utilized for the detection and assessment of soil moisture (Babaeian et al., 2019). Optical images, thermal images, active microwave, and passive microwave data from remote sensing systems are employed to determine soil moisture levels (Babaeian et al., 2019). All image-derived parameters acquired from various satellites have advantages and disadvantages.

Specific indices are occasionally used to extract particular land surface properties from satellite images. These indices are derived by processing the image bands collectively and are commonly employed, especially in drought detection. The Normalized Difference Vegetation Index (NDVI), Enhanced Vegetation Index (EVI), and Palmer Drought Severity Index (PDSI) are some of the significant indices frequently utilized in drought detection, yielding successful results (Zargar et al., 2011; Choi et al., 2013; Liu et al., 2020). Previous research has demonstrated that years of drought in a region can be identified by

anomalies in NDVI and EVI measurements ([Mbatha and Xulu, 2018](#); [Qiu et al., 2022](#)). The methodology section provides detailed explanations of various indices. This study employed NDVI, EVI, and PDSI, extensively used in the literature for drought detection, and investigated their correlations.

Turkey, particularly in recent years, has experienced the tangible effects of global climate change, with recurring phenomena such as diminishing water resources, droughts, and flooding disasters becoming regular occurrences ([Turan, 2018](#)). Drought initially manifests its impact in the agricultural sector and then extends to negatively affect other sectors, making early detection and intervention crucial in mitigating its adverse consequences ([Kapluhan, 2013](#)). The water level of Lake Burdur, located in the study region, has been steadily declining, and this can be attributed to both dams constructed on the rivers that supply water to the lake and the region's ongoing drought ([Ayan and Cengil, 2022](#)). In the context of remote sensing studies in the region, the water level between 2009 and 2019 was determined using the Normalized Difference Water Index (NDWI), a spectral index derived from satellite band calculations. The results revealed a reduction in the lake's water area by 17 km<sup>2</sup> between 2009 and 2019 ([Kaya and Kaplan, 2021](#)). In another study conducted by Taş and Akpinar (2021), the conditions of the lakes in the region were investigated using remote sensing and Geographic Information Systems (GIS) methods. According to their findings, based on an analysis of satellite images taken between 1985 and 2021, the water area of Lake Burdur has decreased by nearly 40%. In [16]Çolak et al. (2022), the ecological consequences of drought in Lake Burdur were examined, and the abundance of waterfowl in the Burdur Basin between 1969 and 2020 was discussed. The study observed that the total waterfowl abundance in 2005 had halved by 2020 ([Çolak et al., 2022](#)).

This study aims to assess water losses in Lake Burdur over the past 10 years utilizing satellite images and to examine their relationship with various parameters. The study explores the correlation between average Land Surface Temperature (LST) and average soil moisture levels from 2010 to 2021, as well as their relationship with changes in the lake's water area. What sets this study apart from previous works by Taş and Akpinar (2021) and [34]Kaya and Kaplan (2021) is the calculation of water areas using a supervised classification approach, which provides a comprehensive assessment of the region's land cover. Furthermore, the study delves into the impacts of drought on the land surface, utilizing Normalized Difference Vegetation Index (NDVI), Enhanced Vegetation Index (EVI), and Palmer Drought Severity Index (PDSI), which are image indices derived from different satellite image bands. The study investigates their connection with drought parameters and established values in the literature. The analysis includes the examination of Land Surface Temperatures, soil moisture, NDVI, EVI, PDSI, precipitation values, and changes in the lake area, with the results being discussed in detail.

This study's contributions to the literature can be summarized as follows: (i) areal loss detection accuracy in watersheds using supervised classification, (ii) the relationship between land surface temperatures, soil moisture, NDVI, EVI, PDSI, and precipitation values with drought and water losses and the correlation between them.

## 2. Study area and dataset

The study was conducted around Lake Burdur, located in the Mediterranean region of Turkey. The Lake Burdur basin is often referred to as the 'lakes region' (Ayan and Cengil, 2022). Lake Burdur spans an area of 153 km<sup>2</sup> and boasts a depth of 8.87 meters (Wikipedia, 2022). The lake exhibits extremely high salinity as a result of alluvial deposits (Yiğitbaşıoğlu and Abdullah, 2010). Due to its salinity and the presence of arsenic in the water, Lake Burdur does not support a wide variety of fish species. Nevertheless, it is a pivotal habitat in the country, particularly for bird species (Yiğitbaşıoğlu and Abdullah, 2010). Figure 1 displays the geographic location of the study area on the map.

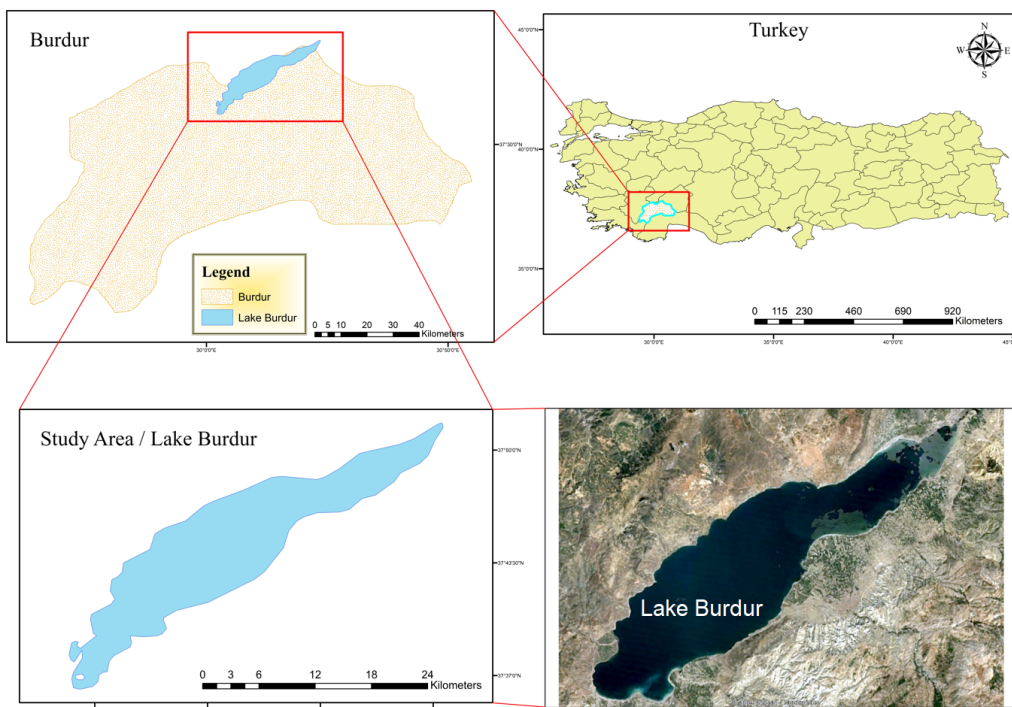


Fig. 1. The study area where Lake Burdur is located

The satellite images used in the study are different for each parameter. Landsat 4-5 and Landsat-8 satellite images, which are freely available from the United States Geological Survey (USGS), were used for supervised classification. The satellite images utilized were taken in 2010, 2013, 2016, 2019, and 2021, respectively. Since Landsat-8 was not yet available in 2010, only Landsat 4-5 satellite imagery for 2010 was used. The satellite images used for supervised classification are given in Figure 2. Table 1 show the bands and wavelength value ranges in the electromagnetic spectrum of the Landsat 4-5 and Landsat 8 satellites, respectively. Moreover, Landsat satellite images were used to calculate NDVI and EVI values. NDVI and EVI are indices frequently used in vegetation

health monitoring. Since drought directly affects vegetation health, NDVI and EVI values were analyzed. Between 2010 and 2021, annual average NDVI and EVI values in the study area were calculated and utilized for the analysis.

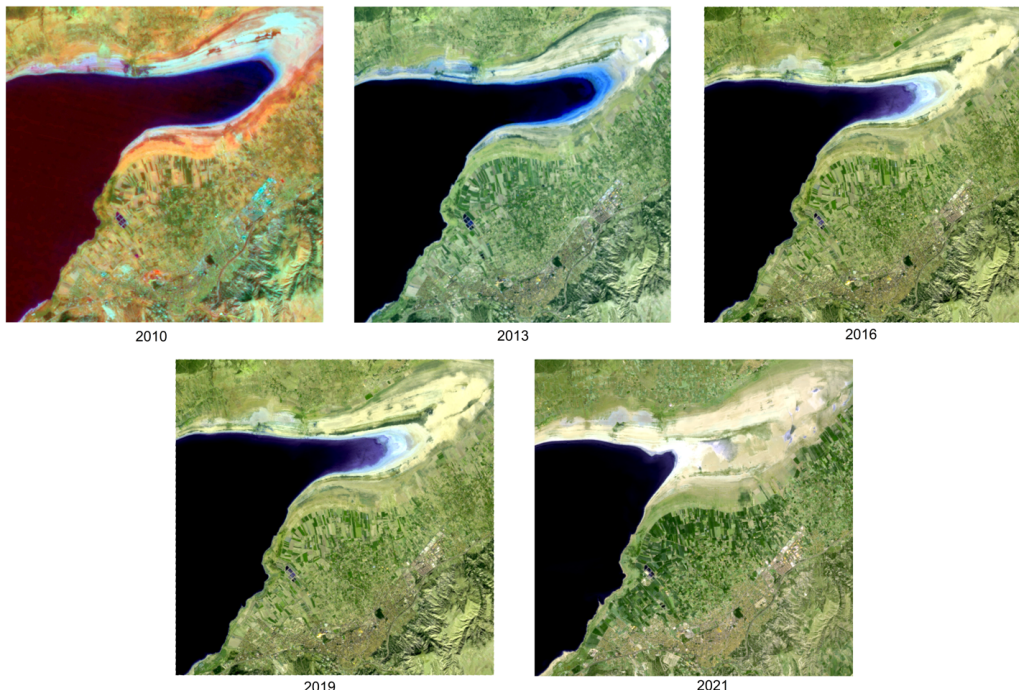


Fig. 2. Satellite images used in the study

As shown in Table 1, Landsat 8 features a greater number of bands compared to Landsat 4-5. For the supervised classification process in this study, the Red, Green, Blue, and Near-Infrared bands, which are common to both satellites, were utilized. In Landsat 8, an additional band was included for coastal and aerosol studies. Moreover, a band for cirrus cloud detection is also present. Landsat 8 also boasts a panchromatic band with a spatial resolution of 15 meters. The scene size of both satellites is equivalent, allowing for their joint analysis. Image acquisition dates and process levels are given in Table 2.

LST values were determined using the MODIS satellite. The National Aeronautics and Space Administration (NASA) launched the MODIS satellite in 1999 and has been providing LST values to the public free of charge since 2000 (Wan, 2008). The MODIS satellite, equipped with 36 different spectral bands, is employed in a wide range of applications, including temperature analysis, agricultural applications, glacier mapping, and disaster monitoring (Hall et al., 2001; Xiao et al., 2006; Vancutsem et al., 2010; Sun et al., 2016). One of the advantages of the MODIS satellite over other thermal band satellites is its ability to collect temperature data from the same location every 8 days, offering sufficient temporal resolution for the study's requirements. Another reason for choosing the MODIS satellite for LST detection is that Landsat 8, which features a thermal

Table 1. Summary of scale factor determinations for tidal gravimeters in the framework of the EPOS-PL and EPOS-PL+ projects

Landsat 4-5	Wavelength ( $\mu\text{m}$ )	Spatial resolution (m)
Band 1 – Blue	0.45–0.52	30
Band 2 – Green	0.52–0.60	30
Band 3 – Red	0.63–0.69	30
Band 4 – Near-Infrared	0.76–0.90	30
Band 5 – Shortwave infrared portions 1	1.55–1.75	30
Band 6 – Thermal	10.40–12.50	120
Band 7 – Shortwave infrared portions 2	2.08–2.35	30
Landsat 8	Wavelength ( $\mu\text{m}$ )	Spatial resolution (m)
Band 1 – Coastal aerosol	0.43–0.45	30
Band 2 – Blue	0.45–0.51	30
Band 3 – Green	0.53–0.59	30
Band 4 – Red	0.64–0.67	30
Band 5 – Near-Infrared	0.85–0.88	30
Band 6 – Shortwave infrared portions 1	1.57–1.65	30
Band 7 – Shortwave infrared portions 2	2.11–2.29	30
Band 8 – Panchromatic	0.50–0.68	15
Band 9 – Cirrus	1.36–1.38	30
Band 10 – Thermal infrared sensor	10.6–11.19	100
Band 11 – Thermal infrared sensor	11.50–12.51	100

Table 2. Image acquisition dates and process levels

Satellite	Image acquisition date	Process level
Landsat 4-5	03.10.2010	C1 – Level 1
Landsat 8	20.05.2013	C1 – Level 1
Landsat 8	22.05.2016	C1 – Level 1
Landsat 8	14.05.2019	C1 – Level 1
Landsat 8	19.05.2021	C1 – Level 1

band and higher spatial resolution, was launched in 2013, making data collection for the years 2010, 2011, and 2012 impossible. Average LST values were gathered in a study area encompassing Lake Burdur over a span of 12 years, beginning in 2010 and concluding in 2021. Additionally, PDSI values were obtained from the TerraClimate dataset, derived from the MODIS satellite (Abatzoglou et al., 2018). The study area was monitored at

short intervals with frequent transitions using the MODIS satellite, known for its high temporal resolution, and PDSI values were computed.

Soil moisture data was collected through collaboration with NASA's Soil Moisture and Ocean Salinity (SMOS) and Soil Moisture Active Passive (SMAP) satellites, in partnership with the United States Department of Agriculture. The SMOS satellite, the first of its kind, was launched to provide explicit soil moisture data (Kerr et al., 2010). With data provided by satellites at 3-day intervals, they offer a high temporal resolution and play a significant role in applications that demand field monitoring (O'Neill et al., 2010). Soil moisture values were extracted from images captured between 2010 and 2021 in the vicinity of Lake Burdur for this study.

### 3. Methodology

The workflow diagram followed in the study is given in Figure 3.

When the workflow diagram is examined in outline, it is seen that it consists of four sections. These are "Data preparation", "Image process", "Analysis of drought parameters" and "Results" respectively. The reason for choosing the study area is discussed in the "Study area and dataset" section. To examine the water loss around Lake Burdur's shore, satellite images were classified. The Maximum Likelihood method was employed for classification. The percentage change in land classes was computed as an outcome of supervised classification. Over a span of 12 years, six different parameters were scrutinized. These parameters were individually analyzed on a monthly basis for each year. The results of these various parameters were subsequently compared using graphical representations. The correlations between the parameters and their relationships to one another were statistically examined using the Spearman rank correlation coefficient method. Finally, the consistency of the results was assessed through Principal Component Analysis (PCA).

The classification method used in this study is the Maximum Likelihood method. A pixel is assigned to a certain class in the Maximum Likelihood technique based on its mean and covariance in the multispectral distribution (Sisodia et al., 2014). Maximum Likelihood classification is widely used in remote sensing applications due to the minimum probability of miscalculation (Pal and Mather, 2003; Kuching, 2007).

The classification process was carried out with the Maximum Likelihood approach for five different years within the scope of the study: 2010, 2013, 2015, 2019, and 2021. For the classification process, five different classes were selected in the study area. The selected classes are Water, Agriculture, Urban Area, Bare Soil, and Sandy, respectively. The classification assessed the changes in the areas of the classes in satellite images according to different years. As a result, the association between changes in water areas and changes in agricultural and sandy areas throughout time was investigated.

The Land Surface Temperature (LST) was calculated using the Google Earth Engine (GEE) platform. GEE provides access to satellite imagery and other data while operating in the cloud, facilitating the processing of large datasets (Kumar and Mutanga, 2018). Due to its continually improving technology and the continuous influx of new data, GEE has found applications in various fields (Mutanga and Kumar, 2019). The LST was derived from

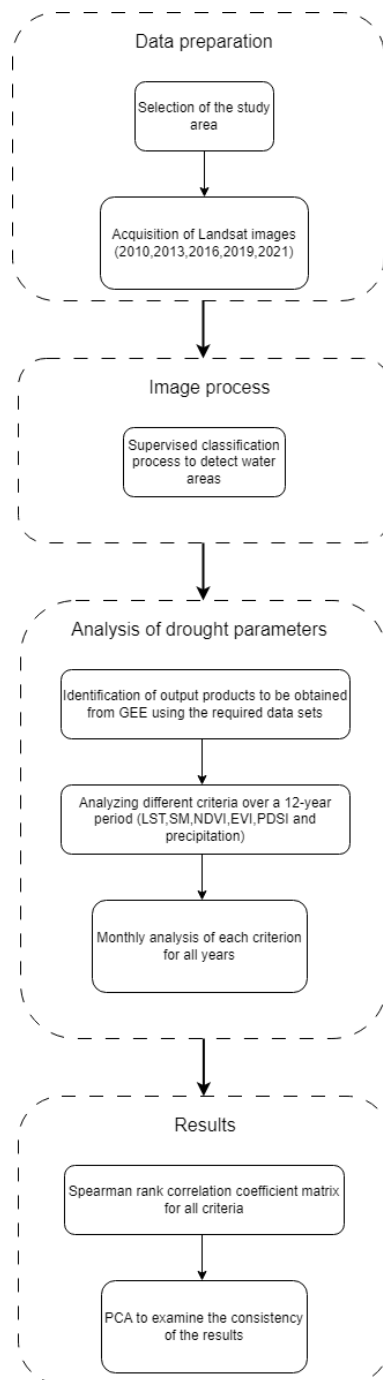


Fig. 3. Workflow of the study

MODIS images, a medium-resolution observation satellite. Each pixel value in the MODIS satellite image represents an 8-day average of land surface temperatures (Wan et al., 2021), resulting in high temporal resolution data suitable for continuous observations. Over a period of 12 years, spanning from 2010 to 2021, average temperature values in the study area were recorded for each year, and their relationships with other parameters were analyzed.

The GEE platform was also used to determine soil moisture values. With the soil moisture data set available in GEE, the number of studies in this field has increased (Sazib et al., 2018). As in the case of land surface temperature data, surface soil moisture was extracted for 12 years between 2010 and 2021 with SMOS and SMAP data around Lake Burdur. The soil moisture values acquired are annual average values, and the relationship with other parameters was examined within the scope of the study.

Drought can be directly related to the state of vegetation on the ground surface (Tucker and Choudhury, 1987). For this reason, it is common to monitor drought with indices derived from bands in satellite imagery (Karnieli et al., 2010; Javed et al., 2021). The NDVI formula is as follows:

$$\text{NDVI} = \frac{\text{NIR} - \text{RED}}{\text{NIR} + \text{RED}}, \quad (1)$$

where *NIR* and *RED* represent the quantities of near-infrared and red light reflected by vegetation and detected by satellite sensors, respectively. NDVI values range from +1 to -1, with negative values indicating a reduction in vegetation density (Myneni et al., 1995).

EVI offers increased sensitivity to regions with high biomass by minimizing soil and atmospheric interferences (Jiang et al., 2008). For this reason, it has been widely employed in drought analysis over the years (Huang et al., 2014; Xie et al., 2021). In areas with significant plant diversity where NDVI may not provide precise results, EVI is used for more accurate verification (Shahzaman et al., 2021). The EVI formula is as follows:

$$\text{EVI} = G \cdot \frac{\text{NIR} - \text{RED}}{(\text{L} + \text{NIR} + C1 \cdot \text{RED} - C2 \cdot \text{BLUE})}, \quad (2)$$

where *L* is the canopy background factor, while *C1* and *C2* are atmospheric correction factors. *G* is a gain factor (Shahzaman et al., 2021). According to official data, if the EVI value is between 0.2 and 0.08, it is assumed that there is drought, while if it is greater than 0.2, it is assumed that there is healthy vegetation (Liu and Huete, 1995). Within the scope of the study, Landsat satellite images taken regularly every month for a period of 12 years were used to determine NDVI and EVI values. PDSI is among the earliest indices to effectively gauge drought severity across various climates (Palmer, 1965). PDSI values span from -4 to +4, with -4 indicating extreme drought and +4 representing extremely wet land conditions (Huang et al., 2011). PDSI takes into account not only soil and water content but also additional factors such as temperature and precipitation. Since the advent of remote sensing technologies, PDSI has been effectively employed in conjunction with other indices to assess drought severity (Bhaga et al., 2020; Mu et al., 2013). In the context of this study, the average PDSI values over 12 years were calculated, and the changes in water areas and their relationships with other parameters were examined in this process.

“Precipitation data” is collected from the Climate Hazards Center at UC Santa Barbara, which provides access to available datasets from the GEE platform. The center regularly offers global precipitation data and has been monitoring droughts since 1981 (Funk et al., 2014).

#### 4. Results

Figure 4 shows the classification results of satellite images for the years 2010, 2013, 2015, 2019, and 2021. In addition, classification accuracies by years are given in Table 3. Table 4 shows the areas of all classes over the years.

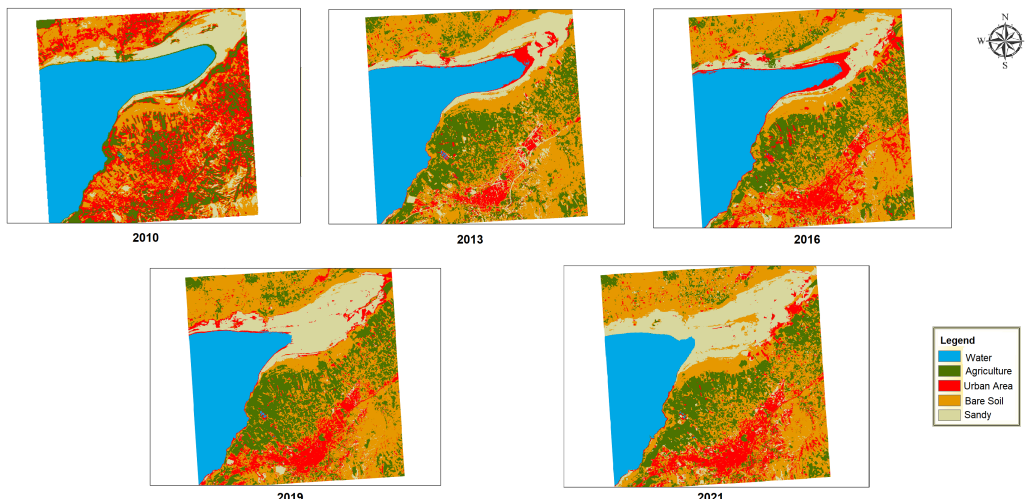


Fig. 4. Result images of classifications

Table 3. Overall accuracies and Kappa Coefficients of the classifications

Year	Overall Accuracy (%)	Kappa Coefficient
2010	79.31	0.74
2013	90.16	0.87
2016	90	0.87
2019	90	0.86
2021	89.65	0.82

In Figure 4, the urban area appears on the coastline in certain years due to the similarity in pixel values between the sandy class and the urban area class. Both classes exhibit comparable reflectance under incoming sunlight, leading to potential confusion. When analyzing the land class areas in Table 4 over different years, there is an 11.12% decrease in water areas between 2010 and 2013, a 9.59% decrease between 2013 and 2016, a 14.08%

Table 4. The area of the classes depends on the years

Year	Water (ha)	Agriculture (ha)	Urban Area (ha)	Bare Soil (ha)	Sandy (ha)
2010	4512.43	2304.43	3996.93	3369.57	1537.96
2013	4010.54	3340.23	1197.05	6267.27	2031.13
2016	3659.61	2856.02	2164.10	6637.18	1709.54
2019	3144.45	3443.67	1846.68	5991.84	2384.85
2021	2866.46	2937.75	1820.17	6208.66	2919.86

decrease between 2016 and 2019, and an 8.84% decrease between 2019 and 2021. Overall, the total water area has decreased by 36.48% from 2010 to 2021. In other significant classes for drought detection, sandy areas have increased by 89.85% between 2010 and 2021, while agricultural areas have grown by 27.48% during the same period. In the determination of the annual average LST between 2010-2021 in the same study area, the average temperature maps are given in Figure 5.

The change in water areas on the northern coast of Lake Burdur, which is our study area, is visible in the annual average temperature maps shown in Figure 5, as is the temperature increase in the sandy area in the same region in the following years. Table 5 shows the annual averages of land surface temperature, soil moisture, NDVI, EVI, PDSI, and precipitation around Lake Burdur to analyze the drought data between 2010 and 2021, respectively.

Table 5. Average values of the data used for drought around Lake Burdur between 2010 and 2021

Year	Average Land Surface Temperature (°C)	Average Land Soil Moisture (m <sup>3</sup> /m <sup>3</sup> )	NDVI	EVI	PDSI	Precipitation (mm)
2010	22.3717	9.7041	0.2272	0.2144	0.6563	1.8173
2011	20.0343	8.1819	0.2406	0.2507	0.7178	1.4518
2012	21.8633	10.5458	0.2216	0.2563	0.7656	1.7979
2013	22.0000	10.3182	0.2462	0.2554	0.5732	1.4052
2014	21.6475	11.0446	0.2228	0.2552	0.4593	1.6155
2015	20.7773	8.1497	0.2315	0.2590	0.8883	1.5527
2016	22.6028	8.7311	0.2194	0.2485	0.1312	1.2663
2017	21.6526	10.3184	0.2357	0.2471	0.3278	1.2749
2018	21.7186	10.3428	0.2323	0.2597	0.3303	1.7578
2019	22.2619	10.1354	0.2125	0.2527	0.4297	1.4237
2020	22.4125	8.7029	0.2298	0.2526	0.2717	1.2612
2021	22.7364	6.7875	0.2025	0.2434	0.1291	1.3041

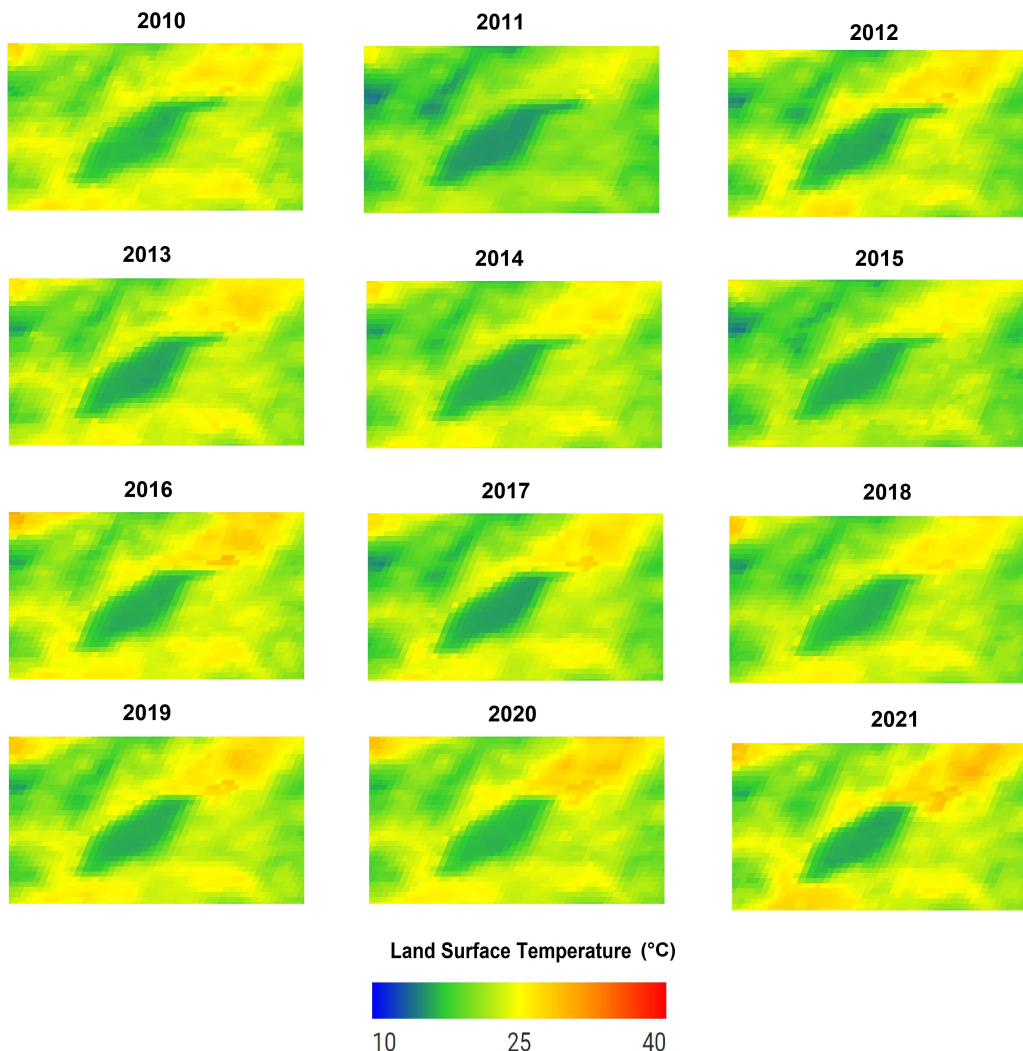


Fig. 5. Map of average land surface temperature values around Lake Burdur between 2010–2021

When the average yearly temperature data were examined, it was discovered that the majority of the highest LST averages were determined in the last 5 years. The highest average temperature value was obtained in 2021 at 22.7364. The lowest average soil moisture value was obtained in 2021 with 6.7875 mm. Looking at the annual average NDVI and EVI values, the lowest NDVI value was 0.2025 in 2021, while the lowest EVI value was 0.2144 in 2010. The lowest EVI value after 2010 was 0.2434 in 2021. Looking at the PDSI values, the lowest PDSI values were obtained in 2016 and 2021. The highest PDSI values were obtained in the period between 2010 and 2015. The variation of the obtained average land surface temperature values according to the months is given in Figure 6.

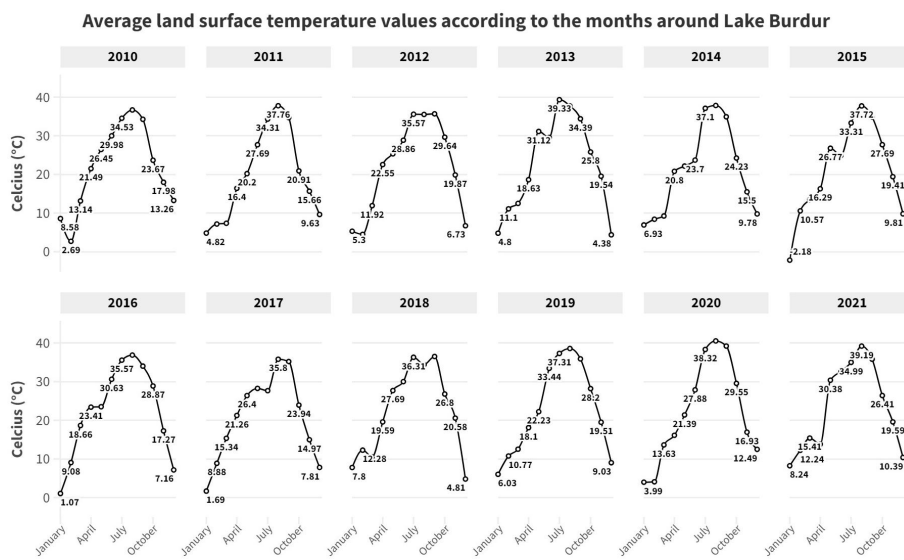


Fig. 6. Average land surface temperature values according to the months around Lake Burdur

When comparing the graphs in Figure 6 with the data in Table 5, it becomes evident that there is a consistent monthly increase in LST values over time. An examination of the monthly data from the annual average LST values presented in Figure 6 reveals that LST has consistently remained at or above approximately 10°C in December, corresponding to the winter months, over the last six years. In prior years, it was observed to be at lower LST values. Furthermore, upon analyzing the graphs, it becomes apparent that rapid temperature fluctuations occur more frequently, particularly in the years 2015 and beyond. The graphs showing the changes in average land soil moisture values during the year are given in Figure 7.

In the graphs of monthly soil moisture values in Figure 7, it was determined that soil moisture values started to increase after October, especially in the 6 years after 2016. In previous years, it was determined that soil moisture increased in earlier months. The graph in which annual the average land surface temperature and annual average soil moisture values in the study region are analyzed together is given in Figure 8.

The graph in Figure 8 shows that temperature values and soil moisture values have a harmonious correlation with each other and that they have increased and decreased inversely in recent years. In 2018 and the following years, LST values increase while SM values decrease as expected. Figure 9 and Figure 10 show the monthly changes in NDVI and EVI values during the year.

Especially when the monthly changes in NDVI values are analyzed, sudden decreases and irregular changes in NDVI values were observed in some months as of 2013. On the other hand, more consistent changes in EVI values were observed within months. However, especially in 2010-2011 and 2012, more intense EVI values in the spring months were detected in the relevant analyzes. Figure 11 shows the monthly changes in PDSI values during the year.

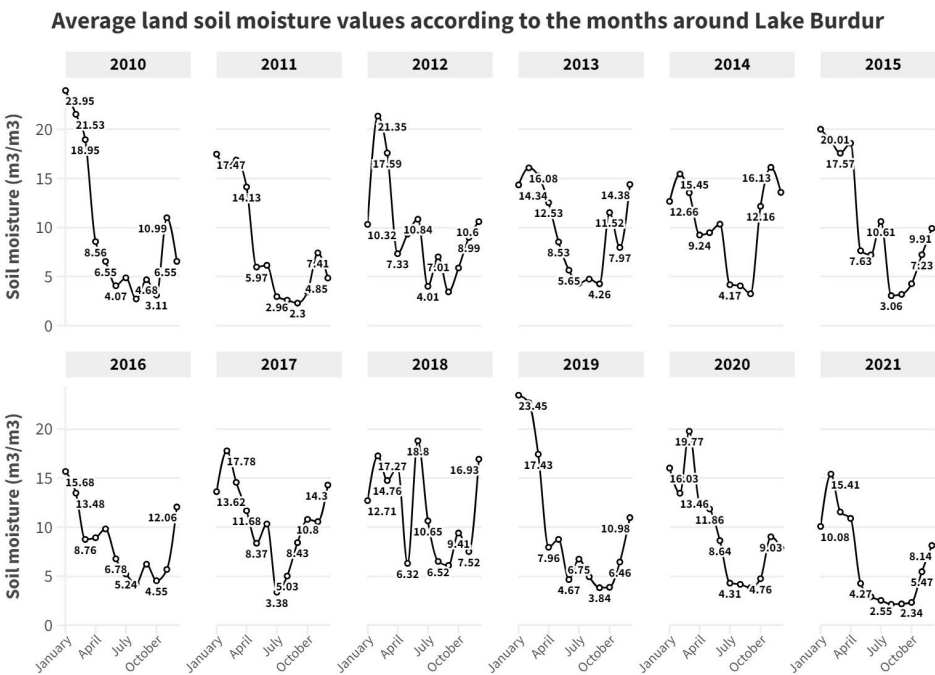


Fig. 7. Average land soil moisture values according to the months around Lake Burdur

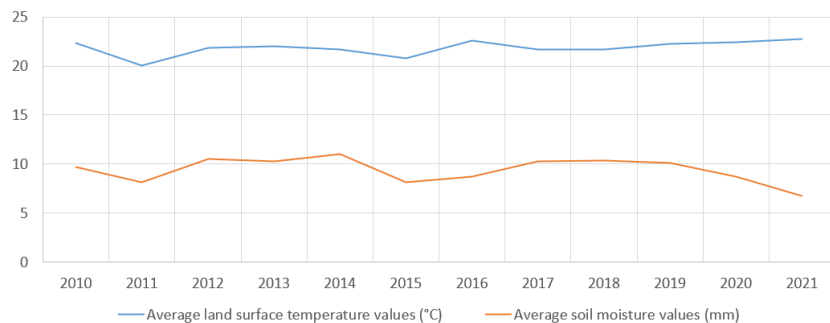


Fig. 8. Annual average temperature values and annual average soil moisture around Lake Burdur

While the PDSI values in Figure 11 do not exhibit significant absolute changes, this is due to the relatively small size of the study region. However, it's important to note that the absolute extreme values for PDSI fall within the range of +4 to -4. Nonetheless, when examining relative comparisons over the years, these offer substantial insights for assessing drought in the study area. An analysis of the monthly PDSI graphs clearly reveals a decrease in values during the year 2016. The graph in Figure 12 shows the monthly change in the amount of precipitation in the study area.

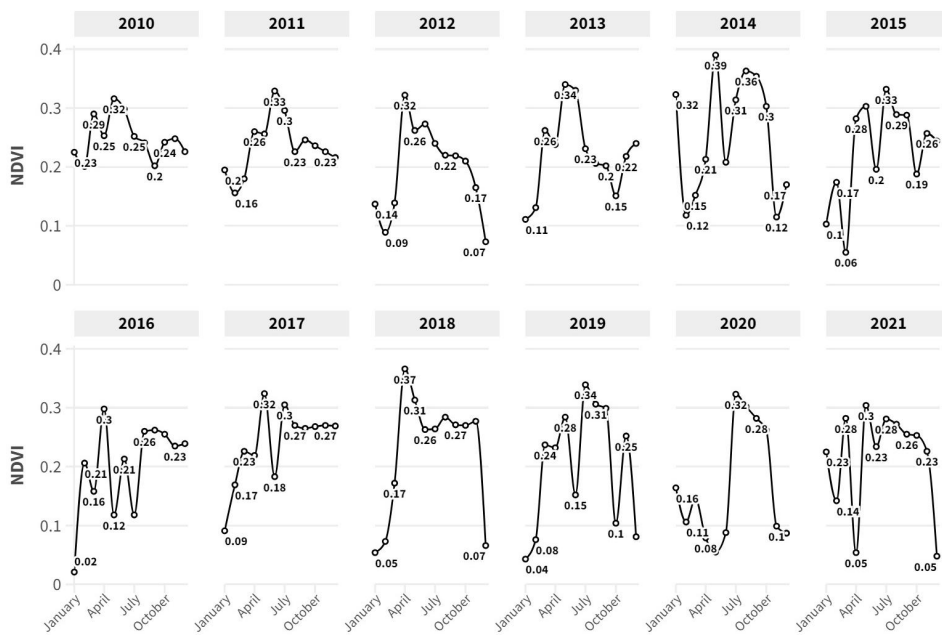
**Average NDVI values according to the months around Lake Burdur**

Fig. 9. Monthly changes of the obtained NDVI values over the years around Lake Burdur

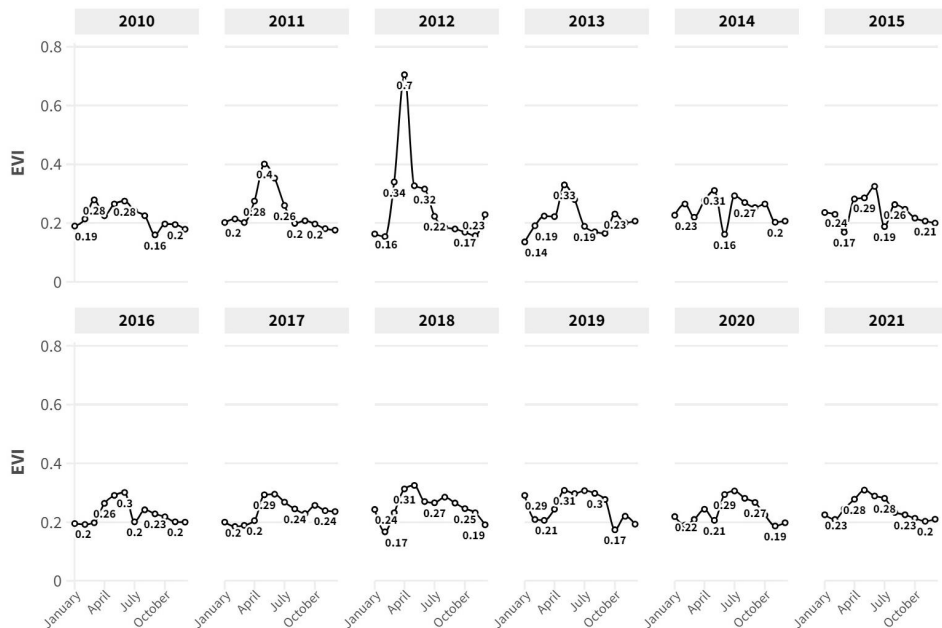
**Average EVI values according to the months around Lake Burdur**

Fig. 10. Monthly changes of the obtained EVI values over the years around Lake Burdur

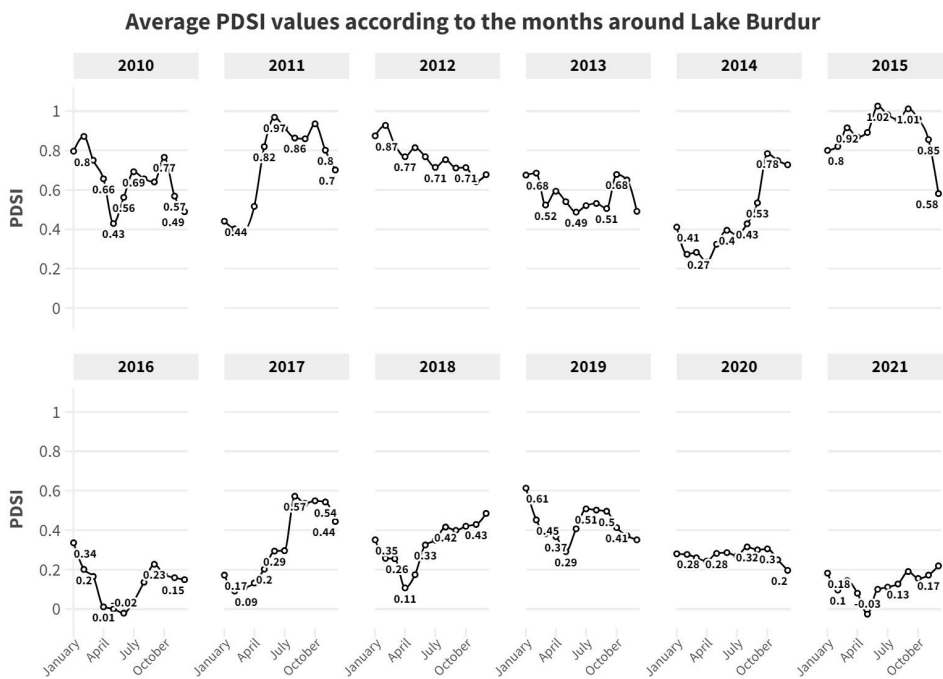


Fig. 11. Monthly changes in PDSI values in the period between 2010-2021 around Lake Burdur

When the precipitation graphs were analyzed, it was determined that the graphs with the lowest precipitation were obtained in the last 6-year period. Figure 13 shows the graph where NDVI, EVI, PDSI and precipitation data are analyzed together according to years.

In Figure 13, the correlation between PDSI and precipitation data is particularly noteworthy and suggests that two different parameters can be evaluated together. The graph clearly shows that the parameters used in drought analysis have decreased since 2015. Figure 14. shows the water areas obtained as a result of the classifications made in Lake Burdur, the study area.

Figure 14 depicts a notable decrease in water areas in the years 2013 and 2019. Upon examining the parameters provided in Table 5, it becomes evident that the amount of precipitation decreased significantly, particularly during the periods of 2012–2013 and 2018-2019. Similarly, it has been observed that LST values have increased compared to previous years, which has reasoned to the alteration in water areas. To determine the correlation between the drought indicators and indices is important to define the implications of drought for the region. In statistics, some methods such as Spearman, Pearson, and Kendall are utilized to compute the pairwise correlation. Specifically, the Spearman rank correlation coefficient demonstrates its superiority over the other methods since it does not need approximate normal distributions of the indicators (Eq. 3) (Bonett and Wrigth, 2000). In Eq. 3,  $\rho$  indicates Spearman's rank correlation coefficient while  $d_i$  and  $n$  represent the difference between the two ranks of each observation and the number

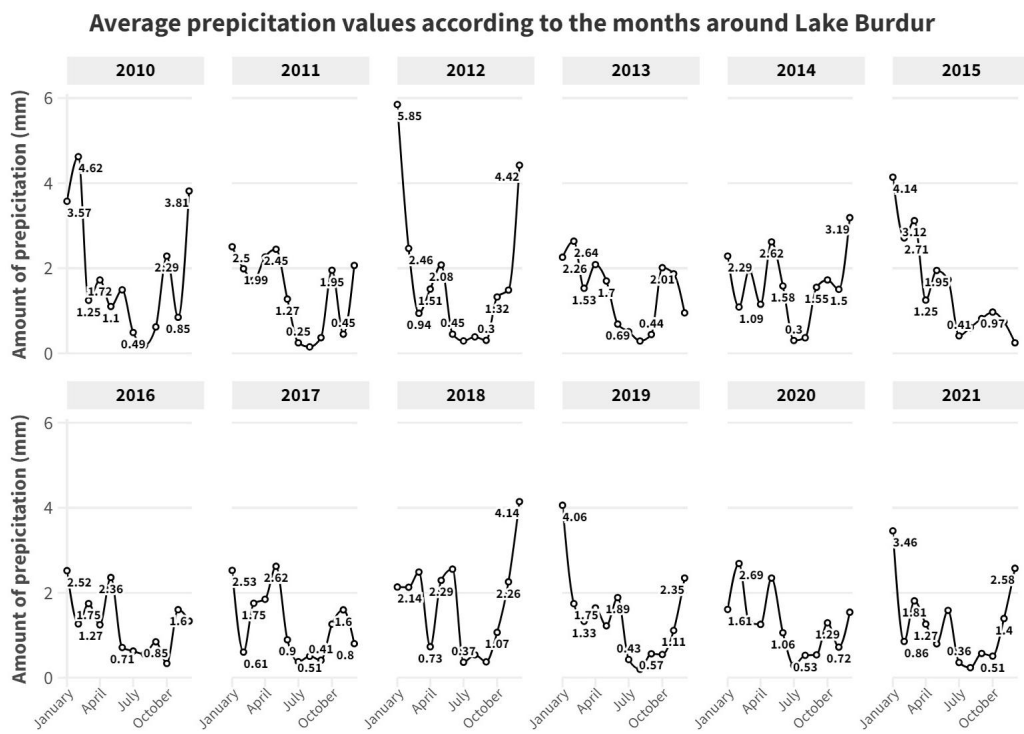


Fig. 12. Monthly changes in precipitation values in the period between 2010–2021 around Lake Burdur

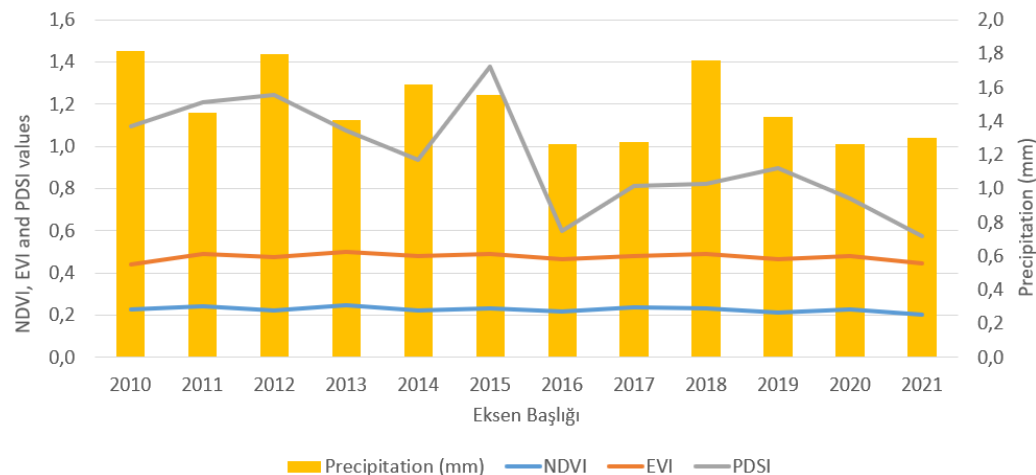


Fig. 13. Annual average of NDVI, EVI, PDSI and precipitation values in the period between 2010–2021 around Lake Burdur

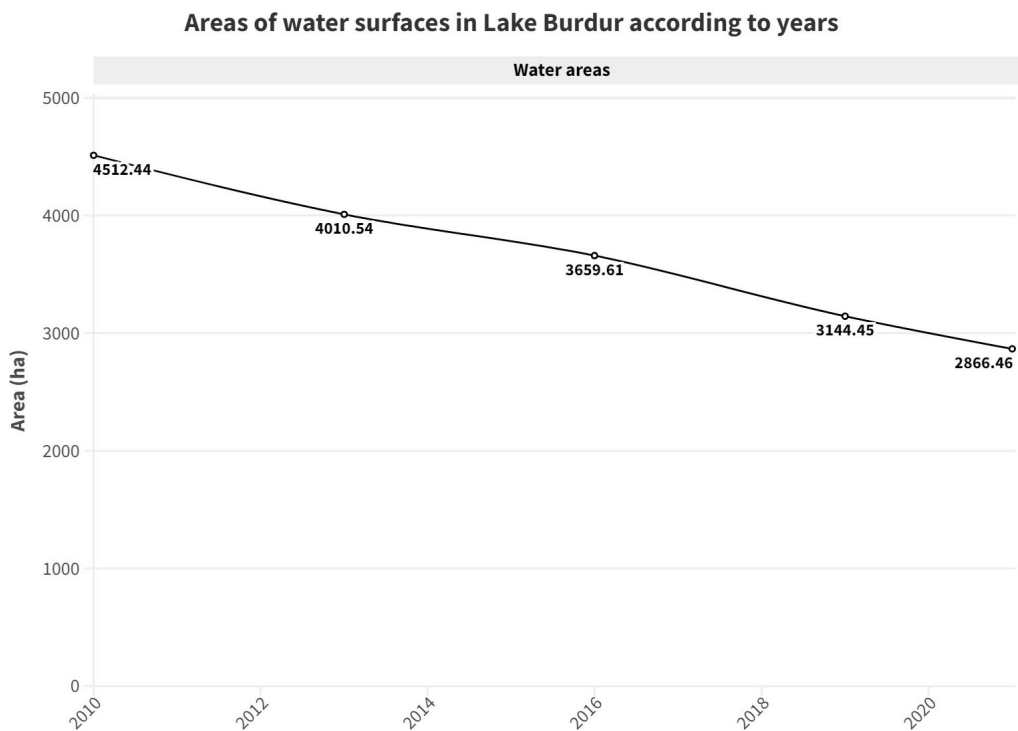


Fig. 14. Areas of water surfaces in Lake Burdur according to years

of observations, respectively. The correlation matrix calculated using the Spearman rank correlation coefficient can be seen in Figure 15. Value of  $-1.0$  indicates a negative correlation, while  $+1.0$  points out a positive correlation between the parameters. When the matrix was examined, surface temperature and soil moisture specify a considerable negative correlation. On the other hand, precipitation and soil moisture present a notable positive correlation:

$$\rho = 1 - \frac{6 \sum d_i^2}{n(n^2 - 1)} . \quad (3)$$

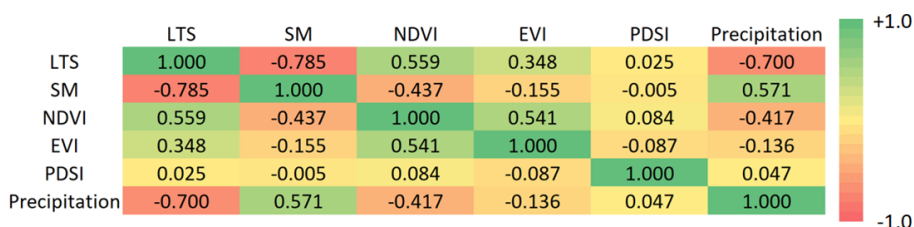


Fig. 15. Visualization of the correlation matrix for the drought parameters

However, the values of the five parameters might contain repetition and inconsistencies to conclude reasonable results about the drought. To reduce data dimension and represent it more abstractly, principal component analysis was applied (Groth et al., 2013). First, the principal components having low eigenvalues were eliminated, and then two significant principal components PC1 and PC2 with 52.4% and 23.1% rational significance values, respectively which can represent 76% of the information were utilized. The eigenvalues  $\lambda_1$  and  $\lambda_2$  of PC1 and PC2 are 0.15334 and 0.06748 respectively. Furthermore, the final two-dimensional dataset was formed using eigenvectors of orthogonal principal components and the drought dataset. When the annual changes in the final two-dimensional dataset were analyzed, an irregularity was explicitly observed, particularly after 2016 (Fig. 16). The figure shows that the second principal component PC2 got negative values in 2016 and after that. It is considered that the abrupt change in 2016 can be one of the indicators of the drought in the lake region.

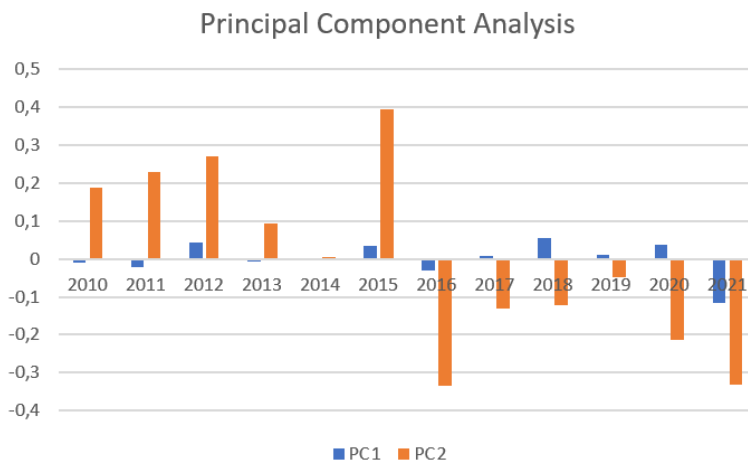


Fig. 16. The temporal distribution of the principal component features

## 5. Summary and conclusions

The land classifications indicate a significant decrease in water areas. The increase in agricultural land and the substantial decrease in water levels over the years suggest that lake water is frequently utilized for agricultural irrigation. Furthermore, the rise in sandy areas over the years is a result of the proliferation of muddy areas caused by the recession of the water level.

When assessing classification accuracies, it becomes apparent that the overall classification accuracy was lower only for the year 2010 compared to other years. This discrepancy can be attributed to the fact that the image for 2010 was acquired using Landsat 4-5 satellites, an earlier series of Landsat satellites, and the reduced spectral resolution of Landsat 4-5 as compared to Landsat 8 contributed to the decline in classification accuracy.

The findings align consistently with prior remote sensing investigations conducted in the respective region in previous years. It has also been revealed that the use of supervised classification algorithms for detecting decreasing areas yields results that are as consistent as those obtained using water indices. When evaluating land surface temperatures over the past 12 years, it becomes evident that the colors representing warmer values in the color palette have intensified in recent years, especially to the north of Burdur Lake, which encompasses our study area. This indicates that changes in water areas may be linked to land surface temperature maps generated by satellites with thermal bands, despite their limited spatial resolution. When we examine individual years for LST, the discrepancies in seasonal temperature fluctuations become apparent. As the image dates approach the present, it is observed that LST is warmer at the beginning of winter and cooler in the spring months. This phenomenon is believed to result in accelerated evaporation during the fall, following precipitation, as well as in the associated lake, which does not receive sufficient replenishment, thereby contributing to the accelerated reduction of water areas.

When examining soil moisture, the second parameter under evaluation in the study, it becomes evident that the average annual values have remained low in recent years. This suggests that the soil is not receiving sufficient moisture, and areas that were once adequately moist are now experiencing a sudden drought. In the course of monthly analysis of soil moisture values over time, it was observed that soil moisture began to increase notably after the mid-autumn months in the early 2010s with the onset of precipitation. However, in recent years, such an increase has occurred in a very brief timeframe before the winter season. This outcome indicates soil drought due to either the insufficient precipitation in the region or the consumption of water from the dam and groundwater, as mentioned in various sources in the literature, through drilling. When considering soil moisture and land surface temperatures together, it is evident that some losses in soil moisture coincide with periods of rising temperatures, as anticipated.

The NDVI and EVI values, which were analyzed as part of the study to enhance vegetation monitoring, did not exhibit significant variations based on the study area's size. However, an examination of yearly values reveals that NDVI values have been lower than in previous years in most cases, particularly after 2015, and these decreases are correlated with the region's drought. In contrast, the lowest EVI values were recorded in 2010 and 2021, indicating a notable threat to vegetation health in the region, particularly in the final year of data collection.

PDSI values, similar to the other parameters, have experienced a significant decline, especially after 2015. When examining PDSI drought values, it is mentioned in the literature that values ranging between 0.5 and 0.99 are generally considered indicative of wet conditions and pose no significant danger, whereas values between 0.49 and -0.99 are viewed as approaching normal conditions. Reviewing the changes in the region, it becomes apparent that there have been years with very low PDSI values since 2015. In accordance with the PDSI ranges, this decline serves as a warning for the upcoming years, signifying that there is very little time remaining before reaching the critical level.

Lastly, when analyzing precipitation levels in the study region, it becomes apparent that the significant rainfall, especially during the autumn months, has decreased over the

past six years, causing drought. Moreover, the synchronized fluctuations of PDSI and precipitation levels in the graphical representation illustrate the close correlation between these two parameters and underscore their significance in drought detection. Compared to various GEE studies, it is notable that [Benzougagh et al. \(2022\)](#) focused on water level monitoring with GEE using NDWI in their research. However, their examination was limited to water areas, and the impact of other land classes in the region on drought was not assessed. In [Zhao et al. \(2021\)](#), the advantages of LST and NDVI data in drought monitoring were discussed, but their effects on water reservoirs were not investigated. The study only presented results from a large-scale worldwide analysis. [Ghazaryan et al. \(2020\)](#) demonstrated that different drought parameters respond differently to drought conditions, but their effects, especially in water areas, were not explored in the study. Their research focused solely on agricultural drought, and the underlying causes were not fully revealed.

## 6. Conclusions

The scope of this study is aimed at determining the changes in water areas in Lake Burdur between 2010 and 2021 and correlating these changes with five drought detection parameters: land surface temperature, soil moisture, NDVI, EVI, PDSI, and precipitation amounts. Landsat images acquired for the years 2010, 2013, 2015, 2019, and 2021 were classified, and both area losses and increases in different land cover classes were identified. Subsequently, yearly average land surface temperatures, soil moisture, NDVI, EVI, PDSI, and precipitation amounts were calculated for the 12-year period from 2010 to 2021 around Lake Burdur. Additionally, monthly variations in these parameters were examined within the study's framework.

When considering all of the findings, significant variations in the parameters used for drought monitoring, especially from 2015 onwards, become apparent. Furthermore, an analysis of land use indicated that water withdrawals supported these findings. This study highlights the advantages of the system implemented on the GEE platform, which can be applied to various locations for data acquisition and analysis. GEE and remote sensing techniques provide rapid results and early warning systems for monitoring various natural disasters, such as drought, thanks to the ever-expanding and updated datasets. This allows for studies covering diverse terrain dynamics at the end-user level.

Lakes, as closed basins, require careful management to maintain water levels. Small river tributaries and precipitation play a crucial role in stabilizing water levels. Additionally, lakes in agricultural regions are often utilized for irrigation. Over time, if more water is used for irrigation than the lake can replenish, the region faces drought, leading to a decline in the lake's water level. If the water level is no longer ecologically sustainable, it can lead to the extinction of the lake's ecosystem. Therefore, monitoring water levels, especially in closed basin lakes, and assessing the parameters that influence these levels are of great significance.

This study demonstrates that decreases in water levels and subsequent area losses can be correlated and used in conjunction with parameters like soil moisture, LST, NDVI, EVI, PDSI, and precipitation. It also emphasizes that supervised classification provides

valuable validation data for identifying areas of decline. If no measures are taken, it is anticipated that the lake will experience a level of drought that could devastate its ecosystems. Therefore, it is essential to record various parameters like PDSI, NDVI, and precipitation amounts, which are scientifically proven for drought detection, for each period and to promptly monitor drought in the region. Under the UN-SDG, active monitoring through satellite imagery plays a critical role in disaster monitoring. Today, with changing climate conditions, the risk of natural disasters is escalating exponentially and poses a significant threat to humanity. Hence, rapid analysis on cloud platforms like GEE, as demonstrated in this study, can help mitigate the impacts of predictable disasters.

## Author contributions

Conceptualization: A.B.P.; methodology: A.B.P., O.A., F.K.; formal analysis and investigation: A.B.P., F.K.; writing – original draft preparation: A.B.P.; writing – review and editing: O.A.; supervision: A.B.P., O.A.

## Data availability statement

The datasets used during the current study are available from the corresponding author on reasonable request.

## Acknowledgements

No funding was obtained for this study.

## References

- Abatzoglou, S., Dobrowski, J.T., Parks, S.A. et al. (2018). Terraclimate, a high-resolution global dataset of monthly climate and climatic water balance from 1958–2015. *Sci. Data*, 5, 170191. DOI: [10.1038/sdata.2017.191](https://doi.org/10.1038/sdata.2017.191).
- Abbasian, M.S., Najafi, M.R., and Abrishamchi, A. (2021). Increasing risk of meteorological drought in the Lake Urmia basin under climate change: Introducing the precipitation–temperature deciles index. *J. Hydrol.*, 592, 125586. DOI: [10.1016/j.jhydrol.2020.125586](https://doi.org/10.1016/j.jhydrol.2020.125586).
- Abburu, S., and Golla, S.B. (2015). Satellite image classification methods and techniques: A review. *Int. J. Comput. Appl.*, 119(8). DOI: [10.5120/21088-3779](https://doi.org/10.5120/21088-3779).
- Abirami, B., Radhakrishnan, M., Kumaran, S. et al. (2021). Impacts of global warming on marine microbial communities. *Sci. Total Environ.*, 791, 147905. DOI: [10.1016/j.scitotenv.2021.147905](https://doi.org/10.1016/j.scitotenv.2021.147905).
- AghaKouchak, A., Farahmand, A., Melton, F.S. et al. (2015). Remote sensing of drought: Progress, challenges and opportunities. *Rev. Geophys.*, 53(2), 452–480. DOI: [10.1002/2014RG000456](https://doi.org/10.1002/2014RG000456).
- Alam, A., Bhat, M.S., and Maheen, M. (2020). Using Landsat satellite data for assessing the land use and land cover change in Kashmir valley. *Environ. Sci.*, 85(6), 1529–1543. DOI: [10.1007/s10708-019-10037-x](https://doi.org/10.1007/s10708-019-10037-x).
- Alfonso, S., Gesto, M., and Sadoul, B. (2021). Temperature increase and its effects on fish stress physiology in the context of global warming. *J. Fish Biol.*, 98(6), 1496–1508. DOI: [10.1111/jfb.14599](https://doi.org/10.1111/jfb.14599).
- Avdan, U., and Jovanovska, G. (2016). Algorithm for automated mapping of land surface temperature using Landsat 8 satellite data. *J. Sensors*, 1480307. DOI: [10.1155/2016/1480307](https://doi.org/10.1155/2016/1480307).

- Ayan, H.Y., and Cengil, B. (2022). Burdur Havzası Kuraklık Yönetimi Değerlendirmesi, In 5th International Symposium on Innovative Approaches in Smart Technologies, Turkey, May 28, 2022. DOI: [10.36287/setsci.5.1.006](https://doi.org/10.36287/setsci.5.1.006) (in Turkish).
- Babaeian, E., Sadeghi, M., Jones, S.B. et al. (2019). Ground, proximal, and satellite remote sensing of soil moisture. *Rev. Geophys.*, 57(2), 530–616. DOI: [10.1029/2018RG000618](https://doi.org/10.1029/2018RG000618).
- Batur, E., and Maktav, D. (2012). Uzaktan Algılama Ve Cbs Entegrasyonu İle Taşkin Alanların Belirlenmesi: Meric Nehri Örneği. *Havacılık ve Uzay Teknolojileri Dergisi*, 5, 47–54. (in Turkish).
- Benzougagh, B., Meshram, S.G., El Fellah, B. et al. (2022). Combined use of Sentinel-2 and Landsat-8 to monitor water surface area and evaluated drought risk severity using Google Earth Engine. *Earth Sci. Inform.*, 15(2), 929–940. DOI: [10.1007/s12145-021-00761-9](https://doi.org/10.1007/s12145-021-00761-9).
- Bhaga, T.D., Dube, T., Shekede, M.D. et al. (2020). Impacts of climate variability and drought on surface water resources in Sub-Saharan Africa using remote sensing: A review. *Remote Sens.*, 12(24), 4184. DOI: [10.3390/rs12244184](https://doi.org/10.3390/rs12244184).
- Bonett, D.G., and Wright, T.A. (2000). Sample size requirements for estimating Pearson, Kendall and Spearman correlations. *Psychometrika*, 65, 23–28. DOI: [10.1007/BF02294183](https://doi.org/10.1007/BF02294183).
- Choi, M., Jacobs, J.M., Anderson, M.C. et al. (2013). Evaluation of drought indices via remotely sensed data with hydrological variables. *J. Hydrol.*, 476, 265–273. DOI: [10.1016/j.jhydrol.2012.10.042](https://doi.org/10.1016/j.jhydrol.2012.10.042).
- Çolak, M.A., Öztaş, B., Özgencil, İ.K. et al. (2022). Increased Water Abstraction and Climate Change Have Substantial Effect on Morphometry, Salinity, and Biotic Communities in Lakes: Examples from the Semi-Arid Burdur Basin (Turkey). *Water*, 14(8), 1241. DOI: [10.3390/w14081241](https://doi.org/10.3390/w14081241).
- Cristóbal, J., Jiménez-Muñoz, J.C., Prakash, A. et al. (2018). An improved single-channel method to retrieve land surface temperature from the Landsat-8 thermal band. *Remote Sens.*, 10(3), 431. DOI: [10.3390/rs10030431](https://doi.org/10.3390/rs10030431).
- Daryanto, S., Wang, L., Jacinthe, P.A. (2016). Global synthesis of drought effects on maize and wheat production. *Plos. One*, 11(5), e0156362. DOI: [10.1371/journal.pone.0156362](https://doi.org/10.1371/journal.pone.0156362).
- Domadia, S.G., and Zaveri, T. (2011). Comparative analysis of unsupervised and supervised image classification techniques. Proceeding of National Conference on Recent Trends in Engineering & Technology, 25–26 February 2011. Kozhikode, Kerala, India.
- Feng, P., Wang, B., Li Liu D. et al. (2019). Machine learning-based integration of remotely-sensed drought factors can improve the estimation of agricultural drought in South-Eastern Australia. *Agric. Syst.*, 173, 303–316. DOI: [10.1016/j.agrysys.2019.03.015](https://doi.org/10.1016/j.agrysys.2019.03.015).
- Funk, C.C., Peterson, P.J., Landsfeld, M.F. et al. (2014). A quasi-global precipitation time series for drought monitoring. US Geological Survey data series, 832(4), 1–12.
- Ghazaryan, G., Dubovyk, O., Graw, V. et al. (2020). Local-scale agricultural drought monitoring with satellite-based multi-sensor time-series. *GISci. Remote Sens.*, 57(5), 704–718. DOI: [10.1080/15481603.2020.1778332](https://doi.org/10.1080/15481603.2020.1778332).
- Godfray, H.C.J., Beddington, J.R., Crute, I.R. et al (2010). Food security: the challenge of feeding 9 billion people. *Sci.*, 327(5967), 812–818. DOI: [10.1126/science.1185383](https://doi.org/10.1126/science.1185383).
- Groth D, Hartmann S, Klie S, Selbig J (2013). Principal Components Analysis. In: Reisfeld, B., Mayeno, A. (eds) Computational Toxicology. Methods in Molecular Biology, vol 930. Humana Press, Totowa, NJ. [https://doi.org/10.1007/978-1-62703-059-5\\_22](https://doi.org/10.1007/978-1-62703-059-5_22).
- Hall, D.K., Riggs, G.A., Salomonson, V.V. et al. (2001). Algorithm theoretical basis document (ATBD) for the MODIS snow and sea ice-mapping algorithms. NASA GSFC, 45. Retrieved September 30, 2022 from [https://tr.wikipedia.org/wiki/Burdur\\_Golu](https://tr.wikipedia.org/wiki/Burdur_Golu).
- Hu, X., Ren, H., Tansey, K. et al. (2019). Agricultural drought monitoring using European Space Agency Sentinel 3A land surface temperature and normalized difference vegetation index imageries. *Agric. Meteorol.*, 279, 107707. DOI: [10.1016/j.agrformet.2019.107707](https://doi.org/10.1016/j.agrformet.2019.107707).

- Huang, S., Dahal, D., Young, C. et al. (2011). Integration of Palmer Drought Severity Index and remote sensing data to simulate wetland water surface from 1910 to 2009 in Cottonwood Lake area, North Dakota. *Remote Sens. Environ.*, 115(12), 3377–3389. DOI: [10.1016/j.rse.2011.08.002](https://doi.org/10.1016/j.rse.2011.08.002).
- Huang, K., Zhou, T., and Zhao, X. (2014). Extreme drought-induced trend changes in MODIS EVI Time Series in Yunnan, China. *IOP Conf. Ser. Earth Environ. Sci.*, 17, 012070. DOI: [10.1088/1755-1315/17/1/012070](https://doi.org/10.1088/1755-1315/17/1/012070).
- Javed, T., Li, Y., Rashid, S. et al. (2021). Performance and relationship of four different agricultural drought indices for drought monitoring in China's mainland using remote sensing data. *Sci. Total Environ.*, 759, 143530. DOI: [10.1016/j.scitotenv.2020.143530](https://doi.org/10.1016/j.scitotenv.2020.143530).
- Jiang, Z., Huete, A.R., Didan, K. et al. (2008). Development of a two-band enhanced vegetation index without a blue band. *Remote Sens. Environ.*, 112(10), 3833–3845. DOI: [10.1016/j.rse.2008.06.006](https://doi.org/10.1016/j.rse.2008.06.006).
- Kapluhan, E. (2013). Türkiye'de kuraklık ve kuraklığın tarıma etkisi. *Marmara Coğrafya Dergisi*, (27), 487–510. (in Turkish)
- Kar, G., and Kumar, A. (2009). Evaluation of post-rainy season crops with residual soil moisture and different tillage methods in rice fallow of eastern India. *Agric. Water Manag.*, 96(6), 931–938. DOI: [10.1016/j.agwat.2009.01.002](https://doi.org/10.1016/j.agwat.2009.01.002).
- Karnieli, A., Agam, N., Pinker, R.T. et al. (2010). Use of NDVI and land surface temperature for drought assessment: Merits and limitations. *J. Clim.* 23(3), 618–633. DOI: [10.1175/2009JCLI2900.1](https://doi.org/10.1175/2009JCLI2900.1).
- Kaya, Ö.A., and Kaplan, G. (2021). Uzaktan Algılama Yöntemleri İle Burdur Gölü'ndeki Alansal Değişiminin Belirlenmesi. *Doğal Afetler ve Çevre Dergisi*, 7(1), 1–12. DOI: [10.21324/dacd.760805](https://doi.org/10.21324/dacd.760805). (in Turkish)
- Kerr, Y.H., Waldteufel, P., Wigneron, J.P. et al. (2010). The SMOS mission: New tool for monitoring key elements of the global water cycle. *Proc. IEEE* 98(5), 666–687. DOI: [10.1109/JPROC.2010.2043032](https://doi.org/10.1109/JPROC.2010.2043032).
- Kuching, S. (2007). The performance of maximum likelihood, spectral angle mapper, neural network and decision tree classifiers in hyperspectral image analysis. *J. Comput. Sci.*, 3(6), 419–423. DOI: [10.3844/jcssp.2007.419.423](https://doi.org/10.3844/jcssp.2007.419.423).
- Kumar, L., and Mutanga, O. (2018). Google Earth Engine applications since inception: Usage, trends, and potential. *Remote Sens.*, 10(10), 1509. DOI: [10.3390/rs10101509](https://doi.org/10.3390/rs10101509).
- Lian, X., Piao, S., Li, L.Z. et al. (2020). Summer soil drying exacerbated by earlier spring greening of northern vegetation. *Sci. Adv.*, 6(1), 0255. DOI: [10.1126/sciadv.aax0255](https://doi.org/10.1126/sciadv.aax0255).
- Liu, H.Q., and Huete, A. (1995). A feedback based modification of the NDVI to minimize canopy background and atmospheric noise. *IEEE Trans. Geosci. Remote Sens.*, 33(2), 457–465. DOI: [10.1109/TGRS.1995.8746027](https://doi.org/10.1109/TGRS.1995.8746027).
- Liu, X., Hu, G., Chen, Y. et al. (2018). High-resolution multi-temporal mapping of global urban land using Landsat images based on the Google Earth Engine Platform. *Remote Sens. Environ.*, 209, 227–239. DOI: [10.1016/j.rse.2018.02.055](https://doi.org/10.1016/j.rse.2018.02.055).
- Liu, Q., Zhang, S., Zhang, H. et al. (2020). Monitoring drought using composite drought indices based on remote sensing. *Sci. Total Environ.*, 711, 134585. DOI: [10.1016/j.scitotenv.2019.134585](https://doi.org/10.1016/j.scitotenv.2019.134585).
- Long, D., Yan, L., Bai, L. et al. (2020). Generation of MODIS-like land surface temperatures under all-weather conditions based on a data fusion approach. *Remote Sens. Environ.*, 246, 111863. DOI: [10.1016/j.rse.2020.111863](https://doi.org/10.1016/j.rse.2020.111863).
- Mbatha, N., and Xulu, S. (2018). Time series analysis of MODIS-Derived NDVI for the Hluhluwe-Imfolozi Park, South Africa: Impact of recent intense drought. *Clim.*, 6(4), 95. DOI: [10.3390/cli6040095](https://doi.org/10.3390/cli6040095).
- Mohammady, M., Moradi, H.R., Zeinivand, H. et al. (2015). A comparison of supervised, unsupervised and synthetic land use classification methods in the north of Iran. *Int. J. Environ. Sci. Technol.*, 12(5), 1515–1526. DOI: [10.1007/s13762-014-0728-3](https://doi.org/10.1007/s13762-014-0728-3).
- Mu, Q., Zhao, M., Kimball, J.S. et al. (2013). A remotely sensed global terrestrial drought severity index. *Bull. Amer. Meteor.*, 94(1), 83–98. DOI: [10.1175/BAMS-D-11-00213.1](https://doi.org/10.1175/BAMS-D-11-00213.1).

- Mutanga, O., and Kumar, L. (2019). Google earth engine applications. *Remote Sens.*, 11(5), 591. DOI: [10.3390/rs11050591](https://doi.org/10.3390/rs11050591).
- Myneni, R.B., Hall, F.G., Sellers, P.J. et al. (1995). The interpretation of spectral vegetation indexes. *IEEE Trans. Geosci. Remote Sens.*, 33(2), 481–486. DOI: [10.1109/TGRS.1995.8746029](https://doi.org/10.1109/TGRS.1995.8746029).
- O'Neill, P., Entekhabi, D., Njoku, E. et al. (2010). The NASA soil moisture active passive (SMAP) mission: Overview. In 2010 IEEE International Geoscience and Remote Sensing Symposium (pp. 3236–3239), 25–30 June 2010. Honolulu, Hawaii, U.S. DOI: [10.1109/IGARSS.2010.5652291](https://doi.org/10.1109/IGARSS.2010.5652291).
- Orhan, O., Ekercin, S., and Dadaser-Celik, F. (2014). Use of landsat land surface temperature and vegetation indices for monitoring drought in the Salt Lake Basin Area, Turkey. *Sci. World J.*, 142939. DOI: [10.1155/2014/142939](https://doi.org/10.1155/2014/142939).
- Pachauri, R.K., Allen, M.R., Barros, V.R. et al. (2014). Climate change 2014: synthesis report. Contribution of Working Groups I, II and III to the fifth assessment report of the Intergovernmental Panel on Climate Change. DOI: [10.1017/epic.45156](https://doi.org/10.1017/epic.45156).
- Pal, M., and Mather, P.M. (2003). An assessment of the effectiveness of decision tree methods for land cover classification. *Remote Sens. Environ.*, 86(4), 554–565. DOI: [10.1016/S0034-4257\(03\)00132-9](https://doi.org/10.1016/S0034-4257(03)00132-9).
- Palmer, W.C. (1965). *Meteorological drought*. US Department of Commerce: Weather Bureau.
- Pan, F., Xi, X., and Wang, C. (2020). A comparative study of water indices and image classification algorithms for mapping inland surface water bodies using Landsat imagery. *Remote Sens.*, 12(10), 1611. DOI: [10.3390/rs12101611](https://doi.org/10.3390/rs12101611).
- Park, S., Seo, E., Kang, D. et al. (2018). Prediction of drought on pentad scale using remote sensing data and MJO index through random forest over East Asia. *Remote Sens.*, 10(11), 1811. DOI: [10.3390/rs10111811](https://doi.org/10.3390/rs10111811).
- Qiu, R., Li, X., Han, G. et al. (2022). Monitoring drought impacts on crop productivity of the US Midwest with solar-induced fluorescence: GOSIF outperforms GOME-2 SIF and MODIS NDVI, EVI, and NIRv. *Agric. Meteorol.*, 323, 109038. DOI: [10.1016/j.agrformet.2022.109038](https://doi.org/10.1016/j.agrformet.2022.109038).
- Rojas, O., Vrieling, A., and Rembold, F. (2011). Assessing drought probability for agricultural areas in Africa with coarse resolution remote sensing imagery. *Remote Sens. Environ.*, 115(2), 343–352. DOI: [10.1016/j.rse.2010.09.006](https://doi.org/10.1016/j.rse.2010.09.006).
- Roy, P., Guha, A., and Kumar, K.V. (2015). An approach of surface coal fire detection from ASTER and Landsat-8 thermal data: Jharia coal field, India. *Int. J. Appl. Earth Obs. Geoinf.* 39, 120–127. DOI: [10.1016/j.jag.2015.03.009](https://doi.org/10.1016/j.jag.2015.03.009).
- Sabuncu, A., Sunar, F. (2017). Ortofotolar ile nesne tabanlı görüntü sınıflandırma uygulaması: Van-Erci Depremi örneği. *Doğal Afetler ve Çevre Dergisi*, 3(1), 1–8. DOI: [10.21324/dacd.271091](https://doi.org/10.21324/dacd.271091). (in Turkish)
- Sazib, N., Mladenova, I., and Bolten, J. (2018). Leveraging the Google Earth Engine for drought assessment using global soil moisture data. *Remote Sens.*, 10(8), 1265. DOI: [10.3390/rs10081265](https://doi.org/10.3390/rs10081265).
- Sazib, N., Bolten, J.D., and Mladenova, I.E. (2021). Leveraging NASA Soil Moisture Active Passive for Assessing Fire Susceptibility and Potential Impacts Over Australia and California. *IEEE J. Sel. Top. Appl. Earth Obs. Remote Sens.*, 15, 779–787. DOI: [10.1109/JSTARS.2021.3136756](https://doi.org/10.1109/JSTARS.2021.3136756).
- Shahzaman, M., Zhu, W., Bilal, M. et al. (2021). Remote sensing indices for spatial monitoring of agricultural drought in South Asian countries. *Remote Sens.*, 13(11), 2059. DOI: [10.3390/rs13112059](https://doi.org/10.3390/rs13112059).
- Shamsuzzoha, M., Noguchi, R., and Ahmed, T. (2021). Damaged area assessment of cultivated agricultural lands affected by cyclone bulbul in coastal region of Bangladesh using Landsat 8 OLI and TIRS datasets. *Remote Sens. Appl. Soc. Environ.*, 23, 100523. DOI: [10.1016/j.rsase.2021.100523](https://doi.org/10.1016/j.rsase.2021.100523).
- Shorachi, M., Kumar, V., and Steele-Dunne, S.C. (2022). Sentinel-1 SAR Backscatter Response to Agricultural Drought in The Netherlands. *Remote Sens.*, 14(10), 2435. DOI: [10.3390/rs14102435](https://doi.org/10.3390/rs14102435).
- Sisodia, P.S., Tiwari, V., and Kumar, A. (2014). Analysis of supervised maximum likelihood classification for remote sensing image. In International conference on recent advances and innovations in engineering (ICRAIE-2014), 9–11 May 2014. Jaipur, India. DOI: [10.1109/ICRAIE.2014.6909319](https://doi.org/10.1109/ICRAIE.2014.6909319).

- Sun, L., Chen, J., and Li, T. (2016). A MODIS-based method for detecting large-scale vegetation disturbance due to natural hazards: a case study of Wenchuan earthquake stricken regions in China. *Stoch. Environ. Res. Risk Assess.*, 30(8), 2243–2254. DOI: [10.1007/s00477-015-1160-z](https://doi.org/10.1007/s00477-015-1160-z).
- Swain, S., Wardlow, B.D., Narumalani, S. et al. (2011). Assessment of vegetation response to drought in Nebraska using Terra-MODIS land surface temperature and normalized difference vegetation index. *GISci. Remote Sens.*, 48(3), 432–455. DOI: [10.2747/1548-1603.48.3.432](https://doi.org/10.2747/1548-1603.48.3.432).
- Trenberth, K.E., Dai, A., Van Der Schrier, G. et al. (2014). Global warming and changes in drought. *Nat. Clim. Chang.*, 4(1), 17–22. DOI: [10.1038/nclimate2067](https://doi.org/10.1038/nclimate2067).
- Tucker, C.J., Choudhury, B.J. (1987). Satellite remote sensing of drought conditions. *Remote Sens. Environ.*, 23(2), 243–251. DOI: [10.1016/0034-4257\(87\)90040-X](https://doi.org/10.1016/0034-4257(87)90040-X).
- Turan, E.S. (2018). Türkiye'nin iklim değişikliğine bağlı kuraklık durumu. *Doğal Afetler ve Çevre Dergisi*, 4(1), 63–69. DOI: [10.21324/dacd.357384](https://doi.org/10.21324/dacd.357384). (in Turkish)
- van Loon, A.F. (2015). Hydrological drought explained. *Wiley Interdiscip. Rev. Water*, 2(4), 359–392. DOI: [10.1002/wat2.1085](https://doi.org/10.1002/wat2.1085).
- Vancutsem, C., Ceccato, P., Dinku, T. et al. (2010). Evaluation of MODIS land surface temperature data to estimate air temperature in different ecosystems over Africa. *Remote Sens. Environ.*, 114(2), 449–465. DOI: [10.1016/j.rse.2009.10.002](https://doi.org/10.1016/j.rse.2009.10.002).
- Varghese, D., Radulović, M., Stojković, S. et al. (2021). Reviewing the potential of Sentinel-2 in assessing the drought. *Remote Sens.*, 13(17), 3355. DOI: [10.3390/rs13173355](https://doi.org/10.3390/rs13173355).
- Vezzulli, L., Pezzati, E., Brettar, I. et al. (2015). Effects of global warming on Vibrio ecology. *Microbiol. Spectr.*, 3(3). DOI: [10.1128/microbiolspec.VE-0004-2014](https://doi.org/10.1128/microbiolspec.VE-0004-2014).
- Wan, Z. (2008). New refinements and validation of the MODIS land-surface temperature/emissivity products. *Remote Sens. Environ.*, 112(1), 59–74. DOI: [10.1016/j.rse.2006.06.026](https://doi.org/10.1016/j.rse.2006.06.026).
- Wan, Z., Hook, S., Hulley, G. (2021). MODIS/Terra Land Surface Temperature/Emissivity 8-Day L3 Global 1km SIN Grid V061 [Data set]. NASA EOSDIS Land Processes DAAC. Retrieved September 10, 2022 from DOI: [10.5067/MODIS/MOD11A2.061](https://doi.org/10.5067/MODIS/MOD11A2.061).
- Wilhite, D.A. (2005). *Drought and water crises: science, technology, and management issues*. Boca Raton: Crc Press. DOI: [10.1201/9781420028386](https://doi.org/10.1201/9781420028386).
- Woolway, R.I., Kraemer, B.M., Lenters, J.D. et al. (2020). Global lake responses to climate change. *Nat. Rev. Earth Environ.*, 1(8), 388–403. DOI: [10.1038/s43017-020-0067-5](https://doi.org/10.1038/s43017-020-0067-5).
- Xiao, X., Boles, S., Frolking, S. et al. (2006). Mapping paddy rice agriculture in South and Southeast Asia using multi-temporal MODIS images. *Remote Sens. Environ.*, 100(1), 95–113. DOI: [10.1016/j.rse.2005.10.004](https://doi.org/10.1016/j.rse.2005.10.004).
- Xie, F., and Fan, H. (2021). Deriving drought indices from MODIS vegetation indices (NDVI/EVI) and Land Surface Temperature (LST): Is data reconstruction necessary?. *Int. J. Appl. Earth Obs. Geoinf.*, 101, 102352. DOI: [10.1016/j.jag.2021.102352](https://doi.org/10.1016/j.jag.2021.102352).
- Yan, F., Qin, Z., Li, M. et al. (2006). Progress in soil moisture estimation from remote sensing data for agricultural drought monitoring. *Remote Sens. Environ. Monitoring, GIS Applications, and Geology*, 6366, 636601. DOI: [10.1111/12.689309](https://doi.org/10.1111/12.689309).
- Yiğitbaşıoğlu, H., and Abdullah, U. (2010). Burdur Gölü havzasında arazi kullanım özelliklerinden kaynaklanan çevre sorunları. *Ankara Üniversitesi Çevrebilimleri Dergisi*, 2(2), 129–143. DOI: [10.1501/Csaum\\_0000000032](https://doi.org/10.1501/Csaum_0000000032). (in Turkish)
- Yiqiang, G., Yanbin, W., Zhengshan, J. et al. (2010). Remote sensing image classification by the Chaos Genetic Algorithm in monitoring land use changes. *Math Comput. Model.*, 51(11-12), 1408–1416. DOI: [10.1016/j.mcm.2009.10.023](https://doi.org/10.1016/j.mcm.2009.10.023).
- Zargar, A., Sadiq, R., Naser, B. et al. (2011). A review of drought indices. *Environ. Rev.*, 19, 333–349. DOI: [10.1139/a11-013](https://doi.org/10.1139/a11-013).
- Zhao, X., Xia, H., Pan, L. et al. (2021). Drought monitoring over Yellow River basin from 2003–2019 using reconstructed MODIS land surface temperature in Google Earth Engine. *Remote Sens.*, 13(18), 3748. DOI: [10.3390/rs13183748](https://doi.org/10.3390/rs13183748).